Scanning magnetoresistance microscopy of atom chips

M. Volk,[a] S. Whitlock,[b] C. H. Wolff, B. V. Hall,[c] and A. I. Sidorov
ARC Centre of Excellence for Quantum-Atom Optics and Centre for Atom Optics and Ultrafast Spectroscopy, Swinburne University of Technology, Hawthorn, Victoria 3122, Australia

(Received 25 April 2007; accepted 7 January 2008; published online 4 February 2008)

Surface based geometries of microfabricated wires or patterned magnetic films can be used to magnetically trap and manipulate ultracold neutral atoms or Bose–Einstein condensates. We investigate the magnetic properties of such atom chips using a scanning magnetoresistive (MR) microscope with high spatial resolution and high field sensitivity. By comparing MR scans of a permanent magnetic atom chip to field profiles obtained using ultracold atoms, we show that MR sensors are ideally suited to observe small variations of the magnetic field caused by imperfections in the wires or magnetic materials which ultimately lead to fragmentation of ultracold atom clouds. Measurements are also provided for the magnetic field produced by a thin current-carrying wire with small geometric modulations along the edge. Comparisons of our measurements with a full numeric calculation of the current flow in the wire and the subsequent magnetic field show excellent agreement. Our results highlight the use of scanning MR microscopy as a convenient and powerful technique for precisely characterizing the magnetic fields produced near the surface of atom chips. © *2008 American Institute of Physics.* [DOI: 10.1063/1.2839015]

I. INTRODUCTION

Surface based potentials for manipulating neutral atoms on a micron scale have attracted widespread interest in recent years. Atom chips[1,2] consisting of planar geometries of microfabricated wires or patterned magnetic materials provide intricate magnetic potentials and have become a practical and robust tool for producing, trapping, and manipulating Bose–Einstein condensates. Atoms chips have recently been used to precisely position Bose–Einstein condensates,[3] realize trapped atom interferometers,[4,5] and have provided new and sensitive techniques for detecting tiny forces on a small spatial scale.[6] The fabricated wires or magnetic materials used for atom chips have been the topic of several recent studies, finding that their quality must be exceptionally high since even the smallest imperfections, for example, roughness of the wire edge, can lead to uncontrolled magnetic field variations. These variations subsequently corrugate the bottom of the trapping potential.[7,8] Recently, fragmentation of ultracold atoms has also been observed in close proximity to magnetic materials[9–11] and has been traced to long range spatial variations in the film magnetization.[10] As the energy scales associated with ultracold atoms and Bose–Einstein condensates are in the nanokelvin regime, even the smallest magnetic field variations of only a few nanotesla can dramatically alter their properties.[12]

Until now, characterizing the smoothness of the potentials produced by atom chips has relied on the atom clouds themselves, through either the equilibrium atomic density distribution[8] or radio frequency spectroscopy of trapped atom clouds.[10] With the increasing complexity of atom chips, however, it is necessary to obtain *fast* and *reliable* methods of characterizing the magnetic potentials prior to installing the atom chips in ultrahigh vacuum and trapping ultracold atoms.

In this paper we describe the application of a micron sized magnetoresistance (MR) sensor to accurately profile the magnetic fields generated by magnetic film and current-carrying wire atom chips. Our home-built magnetoresistance microscope (Fig. 1) is used to measure small magnetic field variations above a permanent magnetic film atom chip which causes fragmentation of ultracold atom clouds. The MR measurements support independent measurements performed using trapped ultracold atoms as the magnetic field probe.[10] The study indicates that the variations occur predominately near the edge of the film and are associated with heating of the film during vacuum bake out. In addition, we have fabricated a new current-carrying wire atom chip using femtosecond laser ablation of a gold film.[13] A wire is sculpted with a periodically modulated edge to produce a complex magnetic potential for ultracold atoms. Two-dimensional images of the field produced by the wire are obtained and are in excellent agreement with numeric calculations of the expected field strength. The measurements show that it is possible to fabricate and characterize a linear array of magnetic potentials produced by modifying the edge of a straight current-carrying wire.

II. APPARATUS

Analysis of the atom chips is performed using an ultrasensitive low-field magnetoresistive sensor based on magnetic tunneling junction (MTJ) technology.[14–16] A magnetic tunneling junction sensor consists of two ferromagnetic lay-

[a]Present address: Solar Systems Pty Ltd., 322 Burwood Road, Hawthorn 3122, Victoria, Australia.
[b]Present address: Van der Waals-Zeeman Instituut, Universiteit van Amsterdam, Valckenierstraat 65-67, 1018 XE Amsterdam, The Netherlands.
[c]Electronic mail: brhall@swin.edu.au.

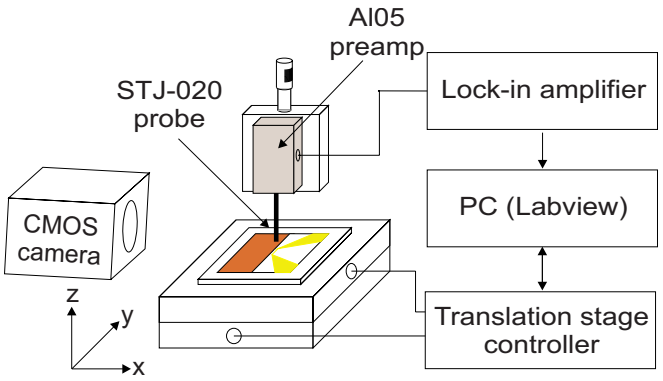

FIG. 1. (Color online) Schematic of the scanning magnetoresistance microscope. The sample is placed on a computer controlled *x*-*y* translation stage. The magnetoresistive probe is connected to a preamplifier and the signal is filtered and digitized by a lock-in amplifier. A CMOS camera is used to determine the distance between the sensor tip and the sample.

ers separated by an ultrathin insulating interlayer. One magnetic layer has fixed "pinned" magnetization while the other responds to the local magnetic field. The interlayer resistance depends on the relative magnetization of the neighboring magnetic layers. These devices provide an absolute measure of the magnetic field with high sensitivity and high spatial resolution. They provide a linear response over a large field range (typically about 0.5 mT) and are ideal for studying the magnetic fields produced by microfabricated current-carrying wires or patterned magnetic materials on atom chips. Here the sensor is incorporated into a home-built scanning magnetic field microscope, schematically depicted in Fig. 1, and used to study the corrugated field produced by the atom chip.

The microscope (Fig. 1) consists of the MR sensor probe, the preamplification electronics, a lock-in amplifier, two motorized translation stages (Thorlabs MT1-Z6) for *x* and *y* positioning and a computer interfaced via LABVIEW to both stage and lock-in amplifier. The probe tip is manually positioned above the sample using a micrometer stage and a complementary metal oxide semiconductor (CMOS) camera for height calibration. The whole system is mounted on an optical table for vibration isolation. This setup allows us to acquire one-dimensional scans as well as two-dimensional maps of the *z*-component, i.e., the out-of-plane component, of the magnetic field at variable heights above the sample surface.

Our scanning magnetoresistance microscope incorporates a commercially available magnetic tunnel junction probe (MicroMagnetics STJ-020), polished to allow very close approaches to the surface (~ 10 μm). The active area of the sensor is approximately 5×5 μm^2 and it detects the magnetic field oriented along the sensor tip (*z* direction). The sensor is interfaced using an Anderson loop[17] to convert small changes in the sensor resistance to a signal voltage which is amplified with a gain of 2500 and a bandwidth of 1 MHz. The Anderson loop and the preamplifier are contained within a signal conditioning board (MicroMagnetics AL-05) which is provided by the sensor manufacturer. Sensor and preamplifier are calibrated to give an output of 20 V/mT. Due to its small size the sensor exhibits significant $1/f$ noise which can be overcome by reducing the bandwidth of the output signal.

To increase the signal-to-noise ratio we use an ac modulation technique. In the case of current-carrying wires this is simply done by modulating the wire current at kilohertz frequencies and detecting the signal with a lock-in amplifier (Stanford Research Systems SR830). When studying permanent magnetic films we use mechanical modulation of the probe. The tip of the probe is oscillated along the scanning direction at its mechanical resonance frequency (18 kHz) using a piezoactuator. At this frequency the noise level of the sensor is reduced to less than 15% compared to dc; however the output of the lock-in amplifier is now proportional to the first derivative of the magnetic field. This output is calibrated against a known magnetic field gradient by first measuring the field in dc mode 200 μm above the edge of the film. The field is large enough to provide good signal-to-noise and features a large gradient of 1 T m^{-1}. We then compare the numerical derivative of this measurement to the data obtained while oscillating the tip. This allows us to determine the oscillation amplitude of the probe and hence to reconstruct the magnetic field up to a constant offset by numerical integration of the data. The oscillation amplitude and subsequently the spatial resolution of this measurement is approximately 50 μm. The ac modulation technique reduces the rms noise levels to about 0.1 μT, equivalent to that obtained using ultracold atoms as a probe[10] and a factor of 5 lower than what is obtained for an equivalent measurement time using just low-pass filtering.

III. PERMANENT MAGNET ATOM CHIP

As a first application of the magnetic field microscope we investigated the random variations in the magnetic potential created near the surface of a magnetic film atom chip used in previous experiments to trap ultracold atoms and Bose–Einstein condensates and is described in detail elsewhere.[18] It uses a multilayer $Tb_6Gd_{10}Fe_{80}Co_4$ film which exhibits strong perpendicular anisotropy. The film is deposited on a 300 μm thick glass substrate where one edge is polished to optical quality prior to film deposition. At this edge the magnetic film produces a field that is analogous to that of a thin current-carrying wire aligned with the edge (I_{eff}=0.2 A). A magnetic microtrap is formed by the field from the film, a uniform magnetic bias field, and two current-carrying end wires. To account for the need of a reflecting surface for the mirror magneto-optical trap the chip is completed by a second glass slide and both sides are coated with gold.

Due to their narrow energy distribution, ultracold atoms are very sensitive to small fluctuations of the magnetic trapping potential. In a recent paper[10] we used radio frequency (rf) spectroscopy of trapped atoms to measure the absolute magnetic field strength above the edge of the film. This provided an accurate measurement of the corrugation of the longitudinal component of the magnetic field produced by the permanent magnetic atom chip, i.e., the component parallel

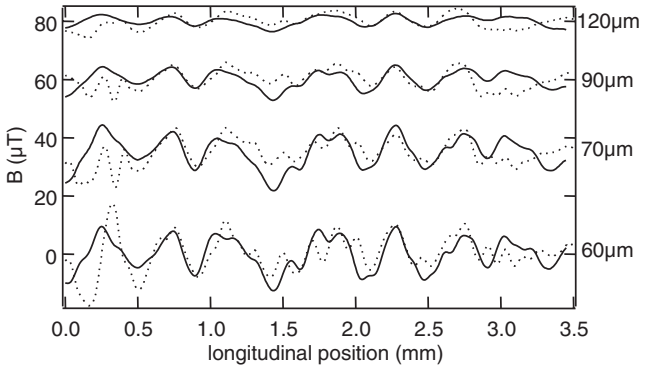

FIG. 2. Magnetic field profiles at various distances above the magnetic film edge of a permanent magnetic atom chip measured with the magnetoresistance microscope sensitive to the B_z field component (solid lines). The dotted lines correspond to measurements of the magnetic field at approximately the same distance using an ultracold atom cloud sensitive to the B_y field component. The profiles have been offset for clarity. The relative longitudinal offset between the two sets of measurements is initially unknown and is adjusted once for optimum agreement.

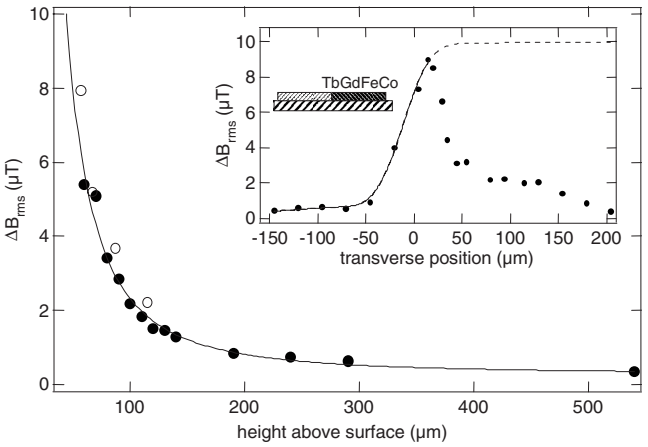

FIG. 3. Behavior of the magnetic field roughness ΔB_{rms} above the film edge measured using the magnetoresistance microscope (filled circles) and rf spectroscopy of ultracold atoms (open circles), as a function of distance from the film surface. The solid line is a power-law fit to the magnetoresistance microscope data. The inset shows the dependence of the field roughness on the transverse distance from the film edge for a fixed height of $z_0=60$ μm above the film surface.

to the film edge. We also developed a model describing the spatial decay of random magnetic fields from the surface due to inhomogeneity in the film magnetization.

After removing the atom chip from the vacuum chamber we used the magnetoresistance microscope to further characterize the film properties. Our first measurement consists of a series of scans of the magnetic field parallel to the film edge over a region of 3.5 mm at various heights ranging from 500 down to 60 μm, the minimum distance limited by the adjacent protruding gold coated glass slide. Four of these profiles are depicted in Fig. 2. Due to the large field gradient produced at the film edge, it was necessary to carefully align the measurement direction and subtract a third order polynomial from the data. Also plotted in the same figure are the corresponding profiles previously measured by rf spectroscopy of ultracold atoms. The results from the two different methods are in remarkable agreement. It should be noted, however, that a quantitative comparison is difficult as the two methods are sensitive to different components of the corrugated magnetic field: the magnetoresistive sensing direction is perpendicular to the surface, while the trap bottom probed by the rf spectroscopy is defined by the in-plane component of the magnetic field.

The results of the complete series of magnetoresistance scans as well as the rf spectroscopy measurements are summarized in Fig. 3 where the root mean square (rms) noise is plotted as a function of distance to the surface. For random white noise fluctuations of the film magnetization our model described in Ref. 10 predicts a z^{-2} decay of the field roughness. A power law fit to the data obtained by the MR scans gives $\Delta B_{\mathrm{rms}} \propto z^{-1.9\pm0.2}$ in excellent agreement with this prediction.

We have also performed a series of scans at constant height ($z_0=60$ μm) above the film surface but variable transverse distance to the film edge. The rms noise levels of these scans are depicted in the inset of Fig. 3 (circles) together with the prediction of the random magnetization model (lines). While the model describes the results adequately above the nonmagnetic half plane of the atom chip the measured inhomogeneity decreases away from the edge above the magnetic film side, whereas in the case of homogeneous magnetization fluctuations ΔB_{rms} is expected to stay constant (dotted line in Fig. 3).

IV. TAILORED MAGNETIC MICROTRAPS

Section III of this paper focused on MR studies of the corrugated potential produced by a partially inhomogeneous magnetic film atom chip. In this section, we describe the analysis of a current-carrying wire atom chip fabricated using micron scale femtosecond laser ablation of a thin metal film. We have produced a tailored magnetic potential by sculpting the shape of a wire to create a linear array of magnetic traps for cold atoms. Two-dimensional magnetoresistance microscopy provides an image of the perpendicular magnetic field component produced by the wire at a fixed distance to the surface. A solution to the magnetostatic inverse problem is then applied to obtain the remaining two field components, allowing a complete reconstruction of the magnetic trapping potential. Of particular interest is the field component parallel to the wire, which defines the bottom of the trapping potential. A comparison of the measured and reconstructed field components with full numeric calculations of the field produced by the sculptured wire shows excellent agreement.

A. Sculptured wire atom chip

Femtosecond laser ablation can be used to pattern micron- and submicron scale structures on a wide variety of materials[19] and can be used to produce atom chips.[13] In this work we use the technique to directly fabricate complex wire patterns in an evaporatively deposited gold film to form a current-carrying wire atom chip.[2] The chip consists of a glass slide substrate with a 25 nm thick Cr bonding layer and a 150 nm thick Au layer. The wire structure is patterned by cutting three 3 μm wide insulating channels into the Au film.

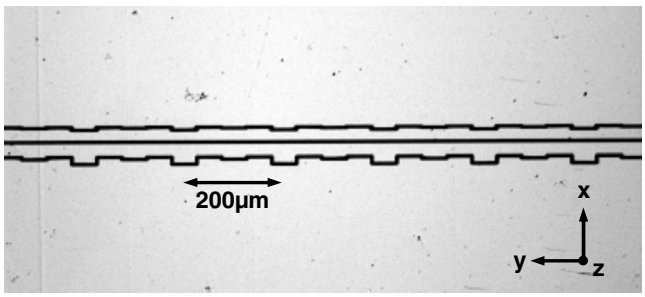

FIG. 4. Optical microscope image of the current-carrying wire atom chip. The two sculptured wires are formed by cutting three 3 μm wide insulating channels, visible as black lines, into a 150 nm thick Au layer using femtosecond laser ablation.

We have patterned two parallel Au wires with widths of 20 and 30 μm and lengths of 10 mm which can be used to create a magnetic potential for trapping Bose–Einstein condensates (Fig. 4). Each wire has been sculptured with one periodically modulated boundary with a period of 200 μm. Deliberately modulating the wire boundary slightly modifies the current path and produces a small field component oriented parallel to the wire, which modulates the corresponding longitudinal magnetic potential experienced by the trapped atoms.[20] This is used to realize a linear array of asymmetric double wells which are separated by potential barriers with small amplitudes which can be precisely controlled by varying the wire current or the distance of the trap to the wire surface.[4,6,21]

The 30 μm wire is chosen for the magnetoresistance measurements. We use the reference source of the lock-in amplifier to drive a small ac current of 37 mA rms through the wire at a frequency of 1 kHz. The output of the lock-in amplifier is recorded by a computer. Two computer controlled translation stages are used to position the wire sample with respect to the MR probe. The probe is calibrated against the expected field produced by the wire calculated using Biot–Savart's law, neglecting the effect of the small modulations. We record an image of the perpendicular magnetic field component produced by the wire over a 2×1.5 mm^2 spatial region at a distance of $z=30$ μm above the wire. The step size is 10 μm which corresponds to 150×200 data points. The lock-in integration time is set to 300 ms and each line of the image is scanned twice and averaged, which results in a measurement time of approximately 5 h for the whole two-dimensional magnetic field image. Figure 5(a) shows the result of this measurement (only the central part of the full image is shown). The field amplitude produced across the wire at this height is ±100 μT. Directly above the wire the perpendicular field is nearly zero apart from a small modulated field component with amplitude of about ±2.5 μT. The rms noise level for this measurement determined from a region about 0.7 mm away from the wire was as low as 50 nT.

B. Reconstruction of the in-plane field components

With a two-dimensional image of the out-of-plane field component at a given height it is possible to convert to an uniquely defined in-plane current distribution[22] and subsequently back to any other field component. Given that the height of the wire is small compared to the measurement distance above the surface, the current density can be considered as a two-dimensional distribution. The Fourier transforms of the magnetic field components b_x and b_y are then simply related to b_z,

$$b_x(k_x,k_y) = i\frac{k_x}{k}b_z(k_x,k_y),$$

$$b_y(k_x,k_y) = i\frac{k_y}{k}b_z(k_x,k_y), \tag{1}$$

where $k=\sqrt{k_x^2+k_y^2}$.

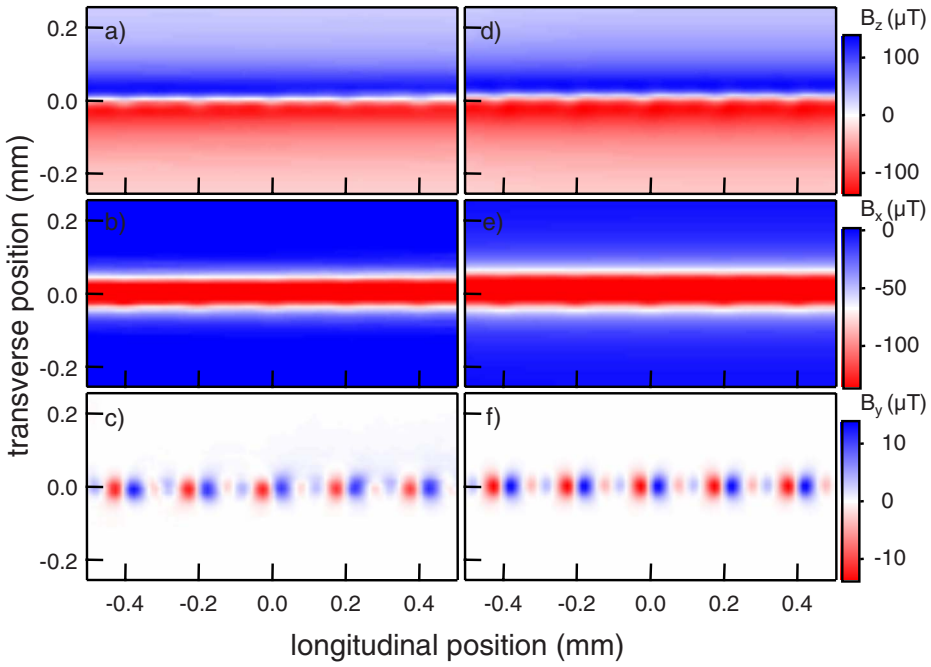

FIG. 5. (Color online) [(a)–(c)] Measured out-of-plane component B_z and reconstructed in-plane components B_x,B_y of the magnetic field above the current-carrying wire atom chip. [(d)–(f)] Corresponding results of the numerical simulation of the current distribution and the associated magnetic field, based on the geometric dimensions of the wire structure.

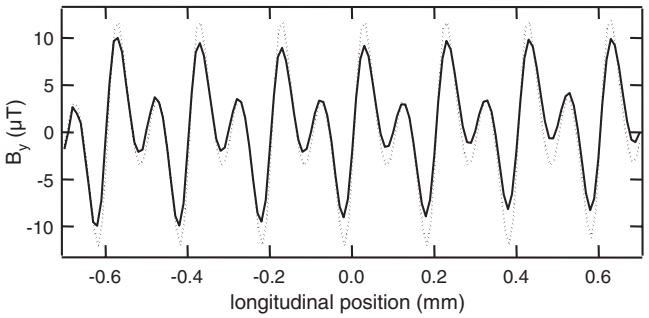

FIG. 6. Line profile of the magnetic field component parallel to the wire (B_y) at $x=0$, i.e., directly above the wire. The solid line represents the field data reconstructed from the MR measurement, while the dotted line shows the simulated values.

Shown in Figs. 5(b) and 5(c) are the reconstructed in-plane field components B_x and B_y derived from the measured B_z component. The B_y field image clearly shows the modulated component along the length of the wire which defines the bottom of the trapping potential.

C. Numeric calculations of magnetic fields

We have also performed detailed numeric calculations of the field produced by the sculptured wire to compare them with our measurements. The current density distribution of the wire is computed from the solution of Laplace's equation $\nabla\cdot(\sigma\nabla V)=0$ satisfied by the electrostatic potential V. We assume that the conductivity σ is uniform throughout the wire and, since we are interested in the field at distances much larger than the wire thickness, we assume that V depends only on x and y. Exact analytical solutions for this problem can be obtained for particular geometries; however, in general, one has to rely on numerical methods.

Here, solutions of Laplace's equation were computed using the finite element method which provides an approximate solution of partial differential equations with defined boundary conditions. For this problem we have used the MATLAB partial differential equation toolbox. The boundary conditions are specified such that the normal component of the current density on the wire edge is zero (Neumann conditions). The wire geometry is then decomposed into a set of triangular elements which define a mesh of nodes, for each of which the electrostatic potential is solved. From this it is straightforward to compute the current distribution and the associated magnetic field. The results of these calculations are depicted in Figs. 5(d)–5(f) next to the corresponding measurements.

The y component of the magnetic field produced by the atom chip is of particular interest because it determines the potential minimum experienced by the trapped atoms. Figure 6 compares field profiles of B_y along the wire extracted from the measurement and the simulation. We note that the two profiles differ by about 10% in amplitude and attribute this to a systematic error in the calibration of the sensor which was done assuming that the measured B_z profile was produced by an infinitely thin wire. In addition to that, the measured field amplitude decreases slightly over the 2 mm scan region which is most likely due to a tilt between the sample surface and the measurement plane on the order of 2 mrad.

Apart from these systematic discrepancies Fig. 5(c) also reveals some irregularities when compared to the simulated magnetic field; thus showing that our system is capable of detecting the small deviation of the field produced by real atom chip from the ideal pattern.

V. DISCUSSION

Two important figures of merit determine the quality of a magnetic field microscope: spatial resolution and field sensitivity. There is a large variety of different magnetic field sensors available.[23] The highest field sensitivity is achieved by superconducting quantum interference device (SQUID) magnetometers with noise levels as low as few $\mathrm{fT}/\sqrt{\mathrm{Hz}}$.[24,25] The spatial resolution of these devices is limited to about 50–100 μm, however[26] and the need for cryogenic cooling makes them less cost effective and easy to use when compared to magnetoresistive sensors. Magnetic force microscopy[27] on the other hand allows the investigation of magnetic structures with a spatial resolution in the nanometer range but with low field sensitivity and results that are difficult to interpret quantitatively.

The need for improved magnetic read heads and better memory elements in magnetic random access memory has driven considerable advances in the development of room temperature magnetoresistive sensors in recent years.[23,28] Applications of these devices include current sensing and fault detection of integrated circuits and MTJ-sensor based magnetic field microscopes with submicron resolution designed for this purpose are commercially available.[29,30] Their spatial resolution is in principle limited by the size of the active area of the probe and the distance between the sensor and the chip surface.

For our demonstration we utilized a probe with an active area of about 5×5 $\mu\mathrm{m}^2$ at a distance of 10 μm between the sensor element and the edge of the probe tip. To prevent damage to the sample as well as the sensor, we operated the microscope in noncontact mode. The minimal distance between the sensor and the chip surface and hence the spatial resolution achieved was about 25 μm, which corresponds to the typical distance cold atoms are trapped at during a standard atom chip experiment.[2] Figure 7 shows the scan of a permanent magnetic lattice[31] with a period of 25 μm. The scans are taken at a height of 25 ± 5 μm above the sample surface and the individual groves of the lattice are clearly resolved. Occasional horizontal displacements in the two-dimensional scan result from positioning inaccuracies of the translation stages and are of the order of 1 μm.

The magnetic field sensitivity of magnetoresistive sensors is generally limited by $1/f$ noise for low frequencies up to about 10–50 kHz.[28] It is therefore favorable to use lock-in techniques to measure at higher frequencies. In our measurement of the current-carrying wire atom chip we modulated the wire current at 1 kHz and limited the measurement bandwidth to 0.42 Hz.[32] The single shot rms noise floor of 70 nT achieved in this measurement is in agreement with the noise level of $100\ \mathrm{nT}\sqrt{\mathrm{Hz}}$ at 1 kHz specified by the manufacturer of the sensor.[33] This is a considerable improvement compared to the sensitivity of 0.5 μT we obtained by simple low

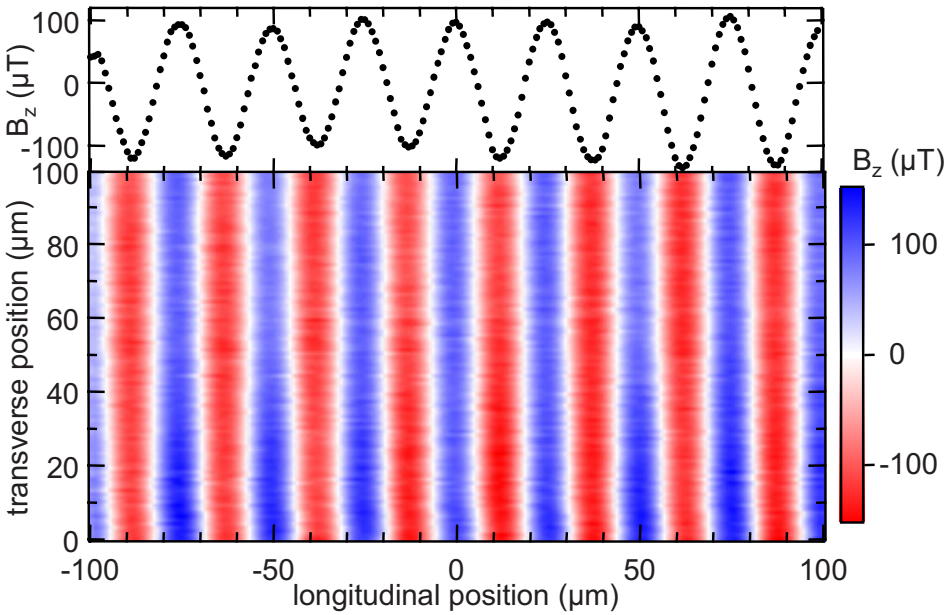

FIG. 7. (Color online) One-dimensional (top) and two-dimensional scans (bottom) of the magnetic field produced by a perpendicularly magnetized permanent magnetic lattice with a period of 25 μm. The scan height and step size for both scans were 25 ± 5 and 1 μm, respectively. Both scans are obtained by recording the low pass filtered output of the sensor in a single pass without averaging.

pass filtering and averaging of the output signal. Measuring at even higher frequencies to further reduce the noise was prevented by the observation that the behavior of the wire started to deviate from that of a pure Ohmic resistance. At this point it is worth mentioning that the $1/f$ noise of MTJ sensors scales as the inverse of the square root of the sensor volume and can be reduced by increasing the lithographically defined size of the sensor element.[30] It should therefore be possible to achieve significantly higher field sensitivity with a specifically designed probe tip tailored to match the desired spacial resolution.

In addition to the intrinsic field noise of the sensor, the magnetic field noise introduced by the translation stages, either through jitter during measurement or through step errors in positioning, is important.[34] Some evidence of this positioning noise can be observed in Fig. 7 which has motivated an upgrade in the MR microscope translation stages to two Newport UTM150pp.1 precision stepper motors which each have a 150 mm range of travel with a 100 nm stepping

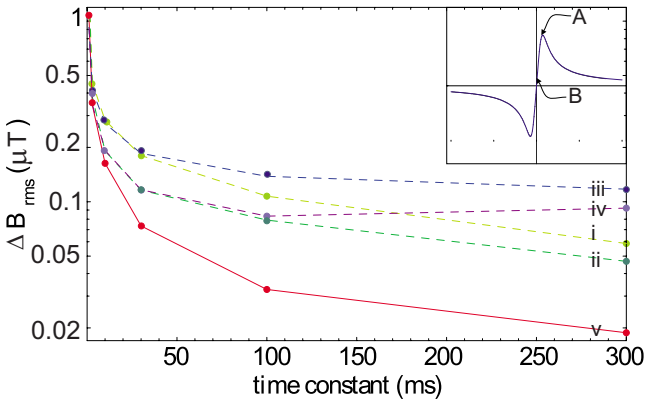

FIG. 8. (Color online) The root mean square deviation of 1000 magnetic field measurements vs integration time (points for data, lines to guide eye). Lines (i) and (ii), sensor stationary at field maximum (inset A) and field gradient maximum (inset B); [(iii) and (iv)], sensor sequentially translating between field maximum (inset A) and field gradient maximum (inset B); (v) background field noise measurement with no wire current.

accuracy. To investigate the positioning noise of these translation stages the rms variation in the magnetic field was derived from 1000 field measurements for a range of integration times between 10 and 300 ms. For each integration time a group of five measurements were made using the ac modulated current and lock-in amplifier (Fig. 8). These five measurements were performed with the sensor *stationary* at the field maximum (i) and the field gradient maximum (ii), with the sensor *translating* sequentially between the field maximum (iii) and the field gradient maximum (iv) and with no current through the wire to measure the background field noise (v). Furthermore, in the translating measurements each time the sensor was brought to rest a pause of five integration times was taken to eliminate biasing of the lock-in amplifier output. Figure 8 indicates that longer integration times continue to reduce the rms deviation of the stationary and background field measurements as expected. For the translating measurements the rms deviation departs from this behavior and asymptotes to a level of approximately 0.1 μT, only a factor of 2 above the intrinsic field noise of the sensor.

VI. CONCLUSION

We have demonstrated a scanning magnetic microscopy technique for characterizing atom chips. The microscope is based on a commercially available magnetoresistive probe. It has been used to scan the corrugation of the magnetic field produced by a permanent magnet atom chip as well as to investigate the field produced by a sculptured current-carrying wire. In conclusion, the high field sensitivity, large scan range, ease of use, and low cost make the magnetoresistance microscope the quintessential tool for *ex situ* characterization of cold atom magnetic microtraps.

ACKNOWLEDGMENTS

The authors would like to thank J. Wang for the deposition of the films. This project is supported by the ARC Centre of Excellence for Quantum-Atom Optics.

[1] R. Folman, P. Krüger, J. Schmiedmayer, J. Denschlag, and C. Henkel, Adv. At., Mol., Opt. Phys. **48**, 263 (2002).
[2] J. Fortágh and C. Zimmermann, Rev. Mod. Phys. **79**, 235 (2007).
[3] A. Günther, M. Kemmler, S. Kraft, C. J. Vale, C. Zimmermann, and J. Fortágh, Phys. Rev. A **71**, 063619 (2005).
[4] T. Schumm, S. Hofferberth, L. M. Andersson, S. Wildermuth, S. Groth, I. Bar-Joseph, J. Schmiedmayer, and P. Krüger, Nature (London) **1**, 57 (2005).
[5] G.-B. Jo, Y. Shin, S. Will, T. A. Pasquini, M. Saba, W. Ketterle, and D. E. Pritchard, Phys. Rev. Lett. **98**, 030407 (2007).
[6] B. V. Hall, S. Whitlock, R. Anderson, P. Hannaford, and A. Sidorov, Phys. Rev. Lett. **98**, 030402 (2007).
[7] D. W. Wang, M. D. Lukin, and E. Demler, Phys. Rev. Lett. **92**, 076802 (2004).
[8] J. Estève, C. Aussibal, T. Schumm, C. Figl, D. Mailly, I. Bouchoule, C. I. Westbrook, and A. Aspect, Phys. Rev. A **70**, 043629 (2004).
[9] C. D. J. Sinclair, J. A. Retter, E. A. Curtis, B. V. Hall, I. Llorente-Garcia, S. Eriksson, B. E. Sauer, and E. A. Hinds, Eur. Phys. J. D **35**, 105 (2005).
[10] S. Whitlock, B. V. Hall, T. Roach, R. Anderson, M. Volk, P. Hannaford, and A. I. Sidorov, Phys. Rev. A **75**, 043602 (2007).
[11] M. Boyd, E. W. Streed, P. Medley, G. K. Campbell, J. Mun, W. Ketterle, and D. E. Pritchard, e-print arXiv:cond-mat/0608370.
[12] S. Wildermuth, S. Hofferberth, I. Lesanovsky, E. Haller, L. M. Andersson, S. Groth, I. Bar-Joseph, P. Krüger, and J. Schmiedmayer, Nature (London) **435**, 440 (2005).
[13] C. H. Wolff, S. Whitlock, M. Lowe, J. Wang, B. V. Hall, A. I. Sidorov, and P. Hannaford, OSA Topical Meeting: Quantum-Atom Optics Downunder, 2007 (unpublished).
[14] J. S. Moodera, L. R. Kinder, T. M. Wong, and R. Meservey, Phys. Rev. Lett. **74**, 3273 (1995).
[15] D. Lacoura, H. Jaffrès, F. N. V. Dau, F. Petroff, A. Vaurès, and J. Humbert, J. Appl. Phys. **91**, 4655 (2002).
[16] X. Liu, C. Ren, and G. Xiao, J. Appl. Phys. **92**, 4722 (2002).
[17] K. F. Anderson, NASA No. TM-104260, 1992, see (http://ntrs.nasa.gov).
[18] B. V. Hall, S. Whitlock, F. Scharnberg, P. Hannaford, and A. Sidorov, J. Phys. B **39**, 27 (2006).
[19] S. Nolte, C. Momma, H. Jacobs, A. Tünnermann, B. N. Chichkov, B. Wellegehausen, and H. Welling, J. Opt. Soc. Am. B **14**, 2716 (1997).
[20] L. D. Pietra, S. Aigner, C. v. Hagen, H. J. Lezec, and J. Schmiedmayer, J. Phys.: Conf. Ser. **19**, 30 (2005).
[21] A. I. Sidorov, B. J. Dalton, S. M. Whitlock, and F. Scharnberg, Phys. Rev. A **74**, 023612 (2006).
[22] B. J. Roth, N. G. Sepulveda, and J. P. Wikswo, Jr., J. Appl. Phys. **65**, 361 (1989).
[23] A. Edelstein, J. Phys.: Condens. Matter **19**, 165217 (2007).
[24] J. R. Kirtley and J. P. Wikswo, Annu. Rev. Mater. Sci. **29**, 117 (1999).
[25] W. G. Jenks, S. S. H. Sadeghi, and J. P. Wikswo, J. Phys. D **30**, 293 (1997).
[26] L. E. Fong, J. R. Holzer, K. K. McBride, E. A. Lima, F. Baudenbachera, and M. Radparvar, Rev. Sci. Instrum. **76**, 053703 (2005).
[27] M. R. Freeman and B. C. Choi, Science **294**, 1184 (2001).
[28] N. A. Stutzke, S. E. Russek, and D. P. Pappas, J. Appl. Phys. **97**, 10Q107 (2005).
[29] B. D. Schrag and G. Xiao, Appl. Phys. Lett. **82**, 3272 (2003).
[30] B. D. Schrag, M. J. Carter, X. Liu, J. S. Hoftun, and G. Xiao, Proceedings of the 32nd International Symposium for Testing and Failure Analysis (ISTFA), 2006, ISBN: 978–0–87170–844–1.
[31] J. Y. Wang, S. Whitlock, F. Scharnberg, D. Gough, A. I. Sidorov, R. J. McLean, and P. Hannaford, J. Phys. D **38**, 4015 (2005).
[32] Equivalent noise bandwidth resulting from a lock-in integration time constant of 300 ms and a low-pass filter slope of 12 dB/oct.
[33] The noise measurement provided in the data sheet of the sensor includes contributions from the Anderson loop and the preamplifier.
[34] S.-Y. Lee, J. Matthews, and F. C. Wellstood, Appl. Phys. Lett. **84**, 5001 (2004).